

SN 2010jp (PTF10aaxi): A Jet-Driven Type II Supernova

Nathan Smith^{1*}, S. Bradley Cenko², Nat Butler², Joshua S. Bloom²,
 Mansi M. Kasliwal³, Assaf Horesh³, Shrinivas R. Kulkarni³, Nicholas M. Law⁴,
 Peter E. Nugent^{2,5}, Eran O. Ofek^{3,6}, Dovi Poznanski^{2,5,6}, Robert M. Quimby³,
 Branimir Sesar³, Sagi Ben-Ami⁷, Iair Arcavi⁷, Avishay Gal-Yam⁷, David Polishook⁷,
 Dong Xu⁷, Ofer Yaron⁷, Dale A. Frail⁸, & Mark Sullivan⁹

¹Steward Observatory, University of Arizona, 933 North Cherry Avenue, Tucson, AZ 85721, USA

²Department of Astronomy, University of California, Berkeley, CA 94720-3411, USA

³Cahill Center for Astrophysics, California Institute of Technology, Pasadena, CA, 91125, USA

⁴Dunlap Institute for Astronomy and Astrophysics, University of Toronto, 50 St. George Street, Toronto M5S 3H4, Ontario, Canada

⁵Computational Cosmology Center, Lawrence Berkeley National Laboratory, 1 Cyclotron Road, Berkeley, CA 94720, USA

⁸Einstein Fellow

⁷The Weizmann Institute of Science, Rehovot 76100, Israel

⁸National Radio Astronomy Observatory, P.O. Box O, Socorro, NM 87801, USA

⁹Department of Physics (Astrophysics), University of Oxford, Keble Road, Oxford, OX13RH, UK

Accepted 0000, Received 0000, in original form 0000

ABSTRACT

We present photometry and spectroscopy of the peculiar Type II supernova (SN) 2010jp, also named PTF10aaxi. The light curve exhibits a linear decline with a relatively low peak absolute magnitude of only -15.9 (unfiltered), and a low radioactive decay luminosity at late times that suggests a low synthesized nickel mass of $M(^{56}\text{Ni}) \lesssim 0.003 M_{\odot}$. Spectra of SN 2010jp display an unprecedented *triple-peaked* $\text{H}\alpha$ line profile, showing: (1) a narrow (FWHM $\gtrsim 800 \text{ km s}^{-1}$) central component that suggests shock interaction with a dense circumstellar medium (CSM); (2) high-velocity blue and red emission features centered at $-12,600$ and $+15,400 \text{ km s}^{-1}$; and (3) very broad wings extending from $-22,000$ to $+25,000 \text{ km s}^{-1}$. These features persist over multiple epochs during the ~ 100 days after explosion. We propose that this line profile indicates a bipolar jet-driven explosion, with the central component produced by normal SN ejecta and CSM interaction at mid and low latitudes, while the high-velocity bumps and broad line wings arise in a nonrelativistic bipolar jet. Two variations of the jet interpretation seem plausible: (1) A fast jet mixes ^{56}Ni to high velocities in polar zones of the H-rich envelope, or (2) the reverse shock in the jet produces blue and red bumps in Balmer lines when a jet interacts with dense CSM. Jet-driven SNe II are predicted for collapsars resulting from a wide range of initial masses above $25 M_{\odot}$, especially at sub-solar metallicity. This seems consistent with the SN host environment, which is either an extremely low-luminosity dwarf galaxy or the very remote parts of an interacting pair of star-forming galaxies. It also seems consistent with the apparently low ^{56}Ni mass that may accompany black hole formation. We speculate that the jet survives to produce observable signatures because the star's H envelope was very low mass, having been mostly stripped away by the previous eruptive mass loss indicated by the Type II_n features in the spectrum.

Key words: ISM: jets and outflows — supernovae: general — supernovae: individual (SN 2010jp)

1 INTRODUCTION

Many theoretical studies of the core-collapse mechanism suggest that breaking spherical symmetry may be an es-

* Email: nathans@as.arizona.edu

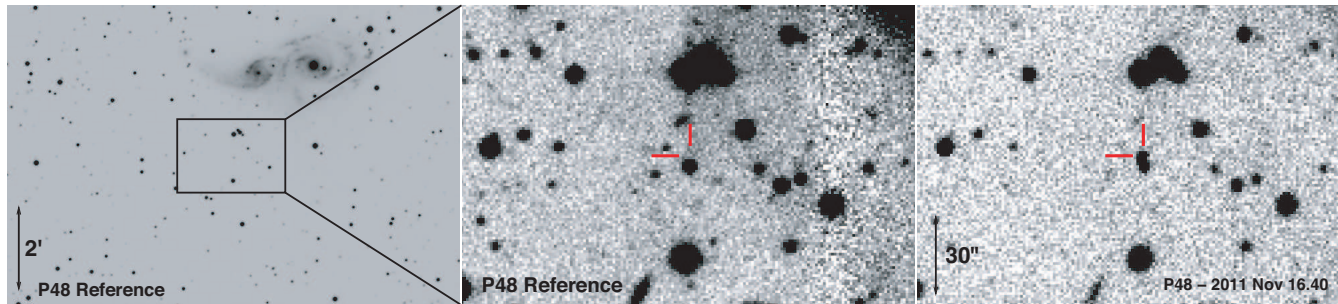


Figure 1. Finder chart for SN 2010jp (PTF10aaxi). *Left:* Wide-field P48 reference image of the SN field, including pre-discovery frames taken from 2009 November to 2010 March. The interacting galaxy pair IC 2163 / NGC 2207, at the same redshift as SN 2010jp, is clearly visible about 2 arcminutes to the north. *Center:* Zoomed-in portion of the same P48 reference image of the location of SN 2010jp. The SN position is indicated with the red tick marks (although the SN itself is not in this image). *Right:* P48 discovery image. The SN position, indicated again with the red tick marks, is only a few arcseconds north of a foreground star, which appears blended with the relatively coarse P48 angular resolution.

sential ingredient in overcoming a stalled shock and producing a successful supernova (SN) explosion (Blondin et al. 2003; Buras et al. 2006a, 2006b; Burrows et al. 2006, 2007). An extreme case of breaking spherical symmetry involves jet-driven explosions (Khokhlov et al. 1999; Höflich et al. 2001; Maeda & Nomoto 2003; Wheeler et al. 2000; Couch et al. 2009). Strongly collimated jets that expel the surrounding stellar envelopes may arise from accretion onto newly-formed black holes as in the “collapsar” model (MacFadyen & Woosley 1999; MacFadyen et al. 2001), or by magnetohydrodynamic (MHD) mechanisms in the collapse and spin-down of highly magnetized and rapidly rotating neutron stars, or magnetars (LeBlanc & Wilson 1970; Bodenheimer & Ostriker 1974; Wheeler et al. 2000; Thompson et al. 2004; Bucciantini et al. 2006; Burrows et al. 2007; Komissarov & Barkov 2007; Dessart et al. 2008; Metzger et al. 2010; Piro & Ott 2011). A jet-driven explosion may be particularly important for producing successful SNe from high-mass stars above $\sim 25 M_{\odot}$ (e.g., MacFadyen et al. 2001; Heger et al. 2003), which might otherwise collapse quietly to a black hole.

The clearest observational evidence for jets in core-collapse SNe comes from the association of broad-lined SNe Ic with the relativistic jets that produce observable gamma-ray bursts (GRBs) (Woosley & Bloom 2006; Galama et al. 1998; Matheson et al. 2003; Mazzali et al. 2005). Launched from deep within the collapsing stellar core, the escape of the jet is facilitated by the fact that the progenitor star was compact and had all of its H envelope (and most or all of its He envelope) stripped away during its prior evolution. Jets are expected to not survive passage through the larger and more massive H envelope of a typical RSG, because jet kinetic energy gets thermalized by the large H envelope (MacFadyen et al. 2001; Höflich et al. 2001). In some cases this scenario may yield a relatively weak explosion powered by accretion onto the black hole (e.g., Quataert & Kasen 2011). An interesting scenario that still needs to be investigated, and which may be central to the present paper, is the behavior of a collimated jet within a small residual H envelope as one might expect in SNe of Types II-L, IIb, or IIc.

Previous evidence for asymmetry in SNe II comes mainly from polarization studies. In two well-studied SNe II-

P, polarization increased while transitioning to the nebular phase, suggesting increasing asymmetry deeper in the expanding ejecta (Leonard et al. 2001, 2006). This seems consistent with increasing levels of polarization with decreasing H envelope mass in different SN types (Trammell et al. 1993; Höflich et al. 1996; Tran et al. 1997; Leonard et al. 2000; Wang et al. 2001; Chornock et al. 2011), whereas the massive H envelope of SN 1987A had weaker polarization (Jeffery 1991 and references therein). A bipolar distribution of ^{56}Ni was also inferred for SN 1999em and SN 2004dj based on blue and red humps in the $\text{H}\alpha$ line profile (Elmhamdi et al. 2003; Chugai et al. 2005); this is similar to the argument we present below for SN 2010jp, but the blue and red humps in SN 2010jp are much faster, more distinct, and are persistent over multiple epochs.

Although there is evidence for some degree of asymmetry seen in some SNe II, there has been no claim of a clear detection of a highly collimated bipolar jet in a SN II. In this paper we discuss kinematic evidence of a jet in a Type II explosion based on the unusual triple-peaked line profiles in optical spectra of SN 2010jp.

2 DISCOVERY AND ENVIRONMENT OF SN 2010jp (PTF10aaxi)

SN 2010jp was discovered on 2010 Nov. 11.3 by Maza et al. (2010), and was found independently on 2010 Nov. 16 as PTF10aaxi in the course of the Palomar Transient Factory (PTF; Law et al. 2009; Rau et al. 2009), as we describe below. Challis, Kirshner, & Smith (2010) obtained a spectrum that showed peculiar line profiles, with narrow peaks in the Balmer lines resembling a Type IIc like SN 2006gy (Smith et al. 2007, 2010; Ofek et al. 2007), but also with very broad line wings extending to at least $\pm 15,000 \text{ km s}^{-1}$ at early times. Throughout, we adopt $E(B-V)=0.087 \text{ mag}$ and $A_R=0.233 \text{ mag}$ as the Galactic reddening and R -band extinction in the direction of SN 2010jp (Schlegel et al. 1998). At $z = 0.009$ measured from the narrow $\text{H}\alpha$ peak in our spectra (see below), we adopt $m - M = 32.9 \text{ mag}$. Corrected for extinction, SN 2010jp then has a peak absolute unfiltered (taken to be approximately R -band) magnitude of -15.9 . This is on the low-luminosity tail of the luminosity

functions for SNe II-L and SNe IIn (Li et al. 2011). In this paper we present additional photometric and spectroscopic observations of SN 2010jp, and we suggest that high-speed material seen in spectra arises in a nonrelativistic jet.

There is no host galaxy known at the position of SN 2010jp. Figure 1 shows an image of the surrounding field. In our pre-explosion PTF images taken between 2009 November and 2010 March, we detected no underlying host galaxy emission to a limiting magnitude of $R > 21.7$ (see below). This may suggest that the host is a very faint and low-metallicity dwarf galaxy with an absolute magnitude fainter than about -12 , roughly 40 times fainter than the Small Magellanic Cloud. Such a faint host is very rare among core-collapse SNe (Arcavi et al. 2010). Alternatively, the position of SN 2010jp is seen about $3'$ in projection from the center of the pair of interacting galaxies NGC 2207/IC 2163 (Figure 1). NGC 2207 has a redshift of $z=0.0091$, which is consistent with that of SN 2010jp. If they are associated, this would put SN 2010jp at a galactocentric radius of about 33 kpc, in the outer regions of this system. This is at the tail of the distribution for host-SN distances among PTF SNe (Kasliwal et al., in prep.). In either case, SN 2010jp occurred in a very low-density and probably also a low-metallicity region, although we do not have any measurement of the true metallicity in the environment. This remote environment may be a key ingredient in producing such an unusual jet-driven SN.

3 OBSERVATIONS

3.1 Palomar 48-inch discovery and photometry

We obtained R -band images of PTF field 100080 on UT 2010 Nov. 16 (UT dates are used throughout) with the Palomar 48-inch telescope (P48) equipped with the refurbished CFHT12k camera (Rahmer et al. 2008). Subtraction of a stacked reference image of the field with HOTPANTS¹ revealed a new transient source at coordinates $\alpha = 06^{\text{h}}16^{\text{m}}30^{\text{s}}.63$, $\delta = -21^{\text{d}}24^{\text{m}}36^{\text{s}}.2$ (J2000.0), with an astrometric uncertainty (relative to the USNO-B1 catalog; Monet et al. 2003) of ± 150 mas in each coordinate. The transient was discovered 30 hours later by Oarical, an autonomous software framework of the PTF collaboration (Bloom et al. 2011b). It was classified correctly as a transient source (as opposed to a variable star), was further classified as a SN or nova, and was given the name PTF10aaxi. This source discovered independently by PTF is the same as SN 2010jp.

No source was detected at this location with P48 in a combined image taken from 2009 November to 2010 March, 8–12 months prior to discovery, to a $3\text{-}\sigma$ limiting magnitude of $R \approx 21.7$ (see Figure 1). The limiting magnitude in the co-added image is actually $R \approx 22.3$ mag, but SN 2010jl is located only a few arcseconds from a bright foreground star that reduces the effective sensitivity of the image at that location.

A listing of P48 observations taken around the time of outburst, calibrated to USNO-B1 R -band (i.e., Vega-based) magnitudes of nearby point sources is provided in Table 1. Because of complications introduced by the nearby star, we

Table 1. P48 R -band magnitudes for SN 2010jp using PSF-fitting photometry.

JD	R mag	R err ^a
2455516.90	18.08	0.02
2455516.95	17.98	0.02
2455517.90	18.01	0.03
2455517.95	17.95	0.02
2455518.80	17.90	0.03
2455530.81	17.90	0.03
2455532.79	18.47	0.03
2455532.83	18.47	0.02
2455533.70	18.74	0.29
2455534.82	18.44	0.04
2455534.83	18.34	0.04
2455535.79	18.60	0.05
2455535.81	18.59	0.13
2455537.77	18.36	0.03
2455537.79	18.38	0.03
2455538.77	18.44	0.03
2455538.81	18.38	0.03
2455558.82	19.04	0.05
2455558.87	19.03	0.04
2455561.76	18.94	0.05
2455561.81	18.88	0.05
2455574.67	19.11	0.11
2455574.72	19.33	0.10
2455575.69	19.08	0.10
2455575.74	19.19	0.09
2455576.70	19.64	0.36
2455576.75	19.50	0.25
2455577.71	19.44	0.26
2455577.75	19.74	0.30
2455578.79	19.09	0.21
2455579.76	19.76	0.13
2455579.81	19.56	0.15
2455583.71	19.48	0.11
2455583.75	19.64	0.14
2455584.70	19.66	0.10
2455584.75	19.61	0.13
2455585.71	19.77	0.12
2455585.76	19.71	0.14
2455587.67	19.41	0.08
2455587.72	19.47	0.10
2455588.73	19.68	0.11
2455588.78	19.88	0.28
2455591.75	19.66	0.07
2455604.67	20.41	0.21
2455605.72	20.79	0.30

^aError bars refer to photon-counting statistics. Uncertainty in the absolute calibration is approximately 0.15 mag.

Table 2. P60 g , r , and i -band magnitudes for SN 2010jp

JD	g mag	g err	r mag	r err	i mag	i err
2455518.87	17.99	0.10
2455529.84	18.50	0.11
2455531.83	18.64	0.11	18.99	0.077
2455532.83	19.25	0.095
2455533.83	18.63	0.11
2455534.85	19.26	0.092	19.02	0.078
2455538.81	18.99	0.079
2455539.81	19.25	0.091	18.58	0.11
2455540.81	18.97	0.081
2455543.80	19.04	0.093	18.50	0.11
2455544.80	18.86	0.084
2455566.74	19.53	0.11
2455567.73	20.02	0.082
2455574.72	20.22	0.094	19.33	0.10	19.93	0.080
2455575.82	20.11	0.097	19.43	0.11	19.83	0.081
2455586.76	20.60	0.093	19.65	0.11	20.34	0.082
2455590.67	20.49	0.092	20.21	0.079
2455591.67	19.84	0.11

¹ <http://www.astro.washington.edu/users/becker/hotpants.htm>

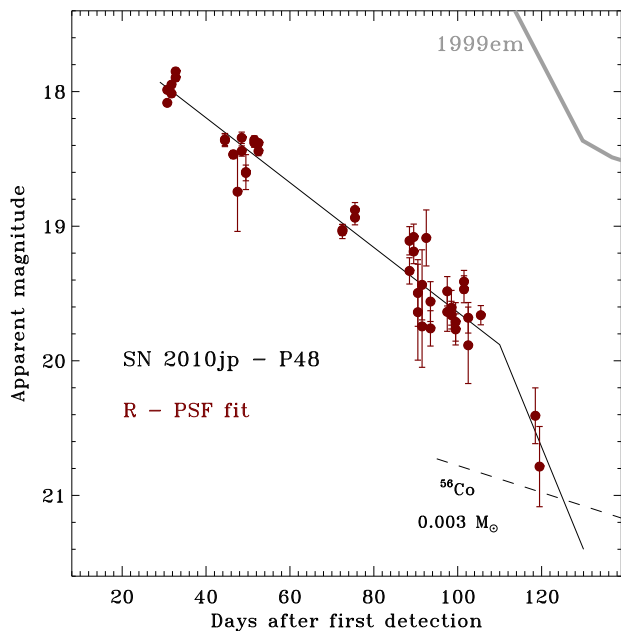


Figure 2. P48 photometry of SN 2010jp, plotted as days after the first detection. We show R -band magnitudes from the Palomar 48-in telescope, reduced using PSF-fitting photometry. The error bars are from photon counting statistics, but the scatter suggests that the true uncertainty is somewhat larger due to systematic effects associated with the bright nearby star. Therefore, the solid black line shows an idealized decline with a fading rate of 0.024 mag d^{-1} until day 110, and a faster fading rate of 0.076 mag d^{-1} after day 110. The dashed line shows the expected ^{56}Co radioactive decay luminosity for $M(^{56}\text{Ni}) = 0.003 M_{\odot}$, and the gray line in the upper right corner is SN 1999em as it would look at the same distance and reddening (see Figure 3).

analyzed the photometry of SN 2010jp using a PSF-fitting routine for the photometry. In each image frame, the PSF is determined from nearby field stars, and this average PSF is then fit at the position of the SN event weighting each pixel according to Poisson statistics, yielding a SN flux and flux error. The resulting magnitudes are given in Table 1 and are shown in Figure 2. We find that photon counting statistics underestimate the uncertainty that is indicated by the observed scatter. We therefore place little emphasis on the minor undulations in the R -band light curve, and instead adopt a representative smooth decline rate shown by the solid line in Figure 2. The last two measurements in Figure 2 were detected with rather large uncertainty. If these late detections are reliable, they imply a somewhat faster rate of fading after day 110.

3.2 Palomar 60-inch photometry

Upon discovery of PTF10aaxi, the field was automatically inserted into the queue of the robotic Palomar 60-inch telescope (P60; Cenko et al. 2006) for multi-colour follow-up observations (Gal-Yam et al. 2011). Images were processed using our custom realtime pipeline, and photometry was performed using a point-spread-function (PSF) matching technique to remove any contribution from the nearby star USNOB-1 0685-0078200. The g' , r' , and i' -band images were

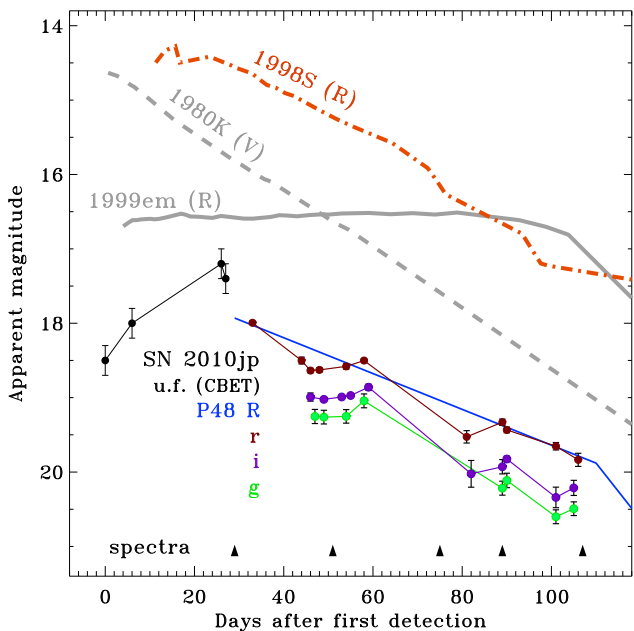


Figure 3. Multi-filter light curve of SN 2010jp, plotted as days after the first detection. We show unfiltered magnitudes taken from preliminary reports (Maza et al. 2010), plus g , r , and i -band photometry from the Palomar 60-in telescope. The solid blue line shows the approximate decline rate of R -band magnitudes from the Palomar 48-in telescope, reproduced from Figure 2. For comparison, we also show the R -band light curves of the normal SN II-P 1999em (Leonard et al. 2002; solid gray line) and the SN II_n 1998S (Fassia et al. 2000; orange dot-dashed line), as well as the V -band light curve of the SN II-L 1980K (Buta 1982; grey dashed line) as they would appear at the same presumed distance of SN 2010jp and with the same assumed foreground extinction. The error bars here and in the data tables reflect photon statistics; the uncertainty in the absolute calibration is somewhat larger, typically 0.15 mag , due to a nearby star. Arrowheads at the bottom denote dates when we obtained spectra of SN 2010jp.

calibrated to USNO-B1 with filter transformations from Jordi et al. (2006), so they are on the SDSS/AB photometric system (Oke & Gunn 1983). A log of our P60 observations of PTF10aaxi is provided in Table 2. The light curve, combining the P48 and P60 photometry, is shown in Figure 3. We also performed an independent analysis of the P60 photometry with the `mkdiff1c` routine (Gal-Yam et al. 2004). The routine uses image subtraction with the common point spread function (PSF) method (CPM, Gal-Yam et al. 2008) for PSF matching. We inserted “artificial” SNe at a similar brightness than that of the real SN, using their post-subtraction magnitude scatter as an estimate of the error due to subtraction residuals. The results (not shown) were comparable to the first analysis of P60 data, although there were differences that exceeded the sizes of error bars. As with the P48 photometry, the nearby star probably increased the observed scatter, so we do not emphasize small scale variation in the P60 light curves. The general rate of fading in P60 gri data is consistent with the P48 R -band data.

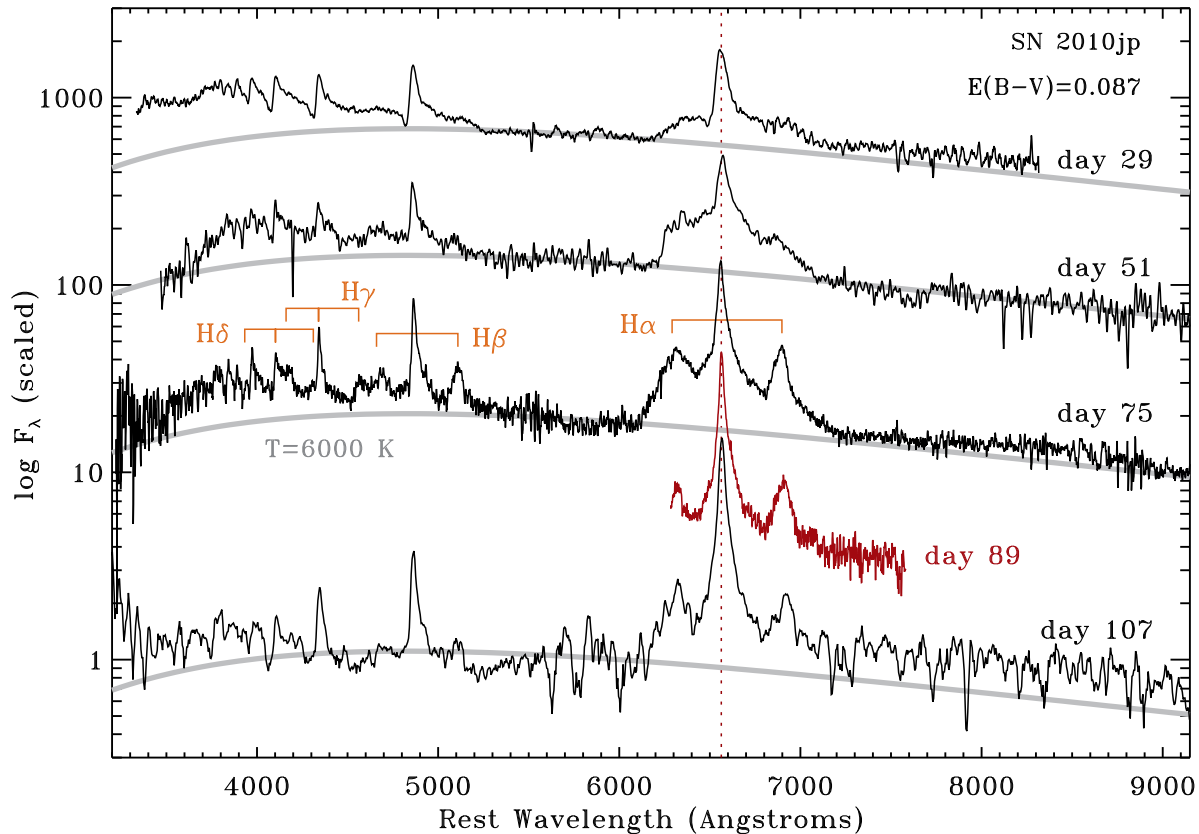


Figure 5. Visual-wavelength spectra of SN 2010jp obtained with the MMT, the Palomar 200-in telescope, and Keck (see Table 3), listed as days after discovery. The day 89 spectrum plotted in red is a high-resolution spectrum from the MMT. The blue and red high-velocity components of H α , H β , H γ , and H δ are marked in orange brackets on the day 75 spectrum.

3.3 *Swift* UV and X-ray Observations

The field of SN 2010jp was observed by the UltraViolet Optical Telescope (UVOT; Roming et al. 2005) on the *Swift* satellite (Gehrels et al. 2004) beginning at 17:01 UT on 2010 November 17. We downloaded the UVOT images from the NASA HEASARC archive², and photometered the images following the recipes provided by Li et al. (2006) (*V*, *B*, and *U*-bands) and Poole et al. (2008) (*UVW1*, *UVM2*, and *UVW2* filters). The resulting measurements are plotted in Figure 4.

Simultaneously, the location of SN 2010jp was observed with the *Swift* X-ray Telescope (XRT; Burrows et al. 2005). We downloaded the XRT observations from the HEASARC archive and reduced individual orbits following the techniques described by Butler (2007). Stacking all available X-ray observations of this location (a total of 28.5 ks of exposure time), no source is detected at the location of SN 2010jp. Assuming a photon spectral index of $\Gamma = 2$, we infer an upper limit on the 0.3–10 keV X-ray flux of $< 1.5 \times 10^{-14}$ erg cm⁻² s⁻¹, or $< 5.0 \times 10^{-4}$ counts s⁻¹.

3.4 EVLA Observations

We observed the field of SN 2010jp using the Expanded Very Large Array (EVLA; Perley et al. 2009) on two separate occasions: 2011 January 11 (C configuration) and 2011 May 12 (BnA configuration). This was part of an observing program entitled “Transients in the Local Universe” (P.I., M. Kasliwal). Both observations were performed in the X-band (8.46 GHz) with a total integration time of 14.0 and 15.4 min on source, respectively, and a total bandwidth of 256 Mhz. The EVLA data were reduced using the Astronomical Image Processing System (AIPS) software.³ The calibration was done using 3C138 as the primary flux calibrator and J0609-1542 as the phase calibrator. A final image was produced using the AIPS IMAGR task with a pixel size of 0'.15. There is no detection at the source position to a 3- σ flux limit of $f_\nu < 48 \mu\text{Jy}$ (Jan. 11) and $f_\nu < 120 \mu\text{Jy}$ (May 12).

3.5 Spectroscopy

After discovery, we obtained several epochs of optical spectroscopy of SN 2010jp using the Bluechannel spectrograph on the 6.5-m Multiple Mirror Telescope (MMT), the Double

² See <http://heasarc.gsfc.nasa.gov>.

³ <http://www.aips.nrao.edu>

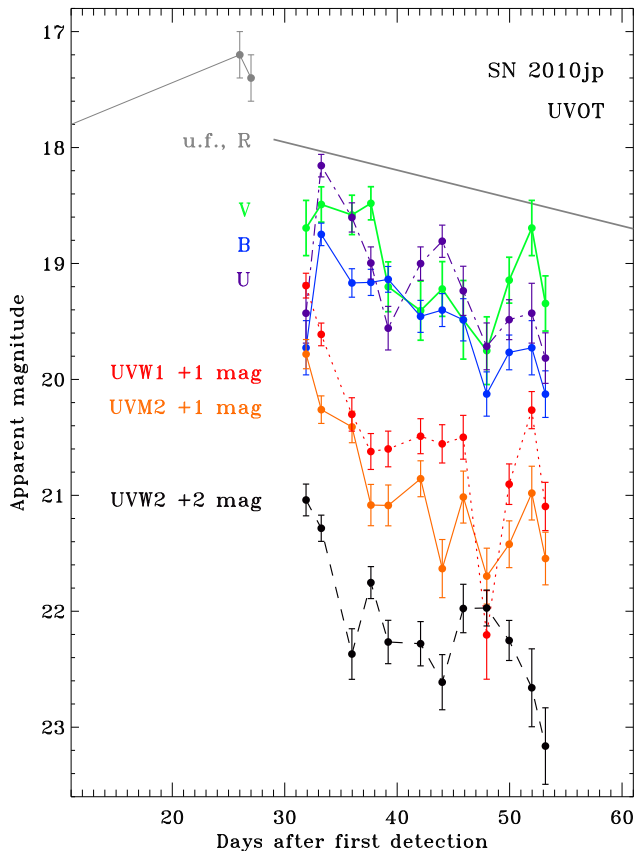


Figure 4. Lightcurves derived from *Swift*/UVOT photometry in the V (green), B (blue), U (purple, dot-dashed line), $UVW1$ (red, dotted line, +1 mag offset), $UVM2$ (orange, +1 mag offset), and $UVW2$ (black, dashed line, +2 mag offset) filters. The unfiltered magnitudes and R -band decline rate from Figure 3 are reproduced in gray for comparison.

Table 3. Spectroscopic observations of SN 2010jp

Date	Tel./Inst.	Day	$\delta\lambda$ (\AA)	$\lambda/\Delta\lambda$	$W_{H\alpha}$ (\AA)
2010 Nov. 14	MMT/B.C.	29	3176–8390	1700	405
2010 Dec. 06	Pal5/DBSP	51	3500–10000	800/500	777
2010 Dec. 30	Keck/LRIS	75	3251–10180	600/1100	1305
2011 Jan. 13	MMT/B.C.	89	6350–7650	4500	...
2011 Jan. 31	Keck/LRIS	107	3100–10220	600/1100	1960

Beam Spectrograph (DBSP; Oke & Gunn 1982) on the Palomar 200-in telescope (P200), and the Low-Resolution Imaging Spectrometer (LRIS; Oke et al. 1995) mounted on the 10-m Keck I telescope. Details of the spectral observations are summarized in Table 3. The slit was always oriented at the parallactic angle (Filippenko 1982), and the long-slit spectra were reduced using standard procedures. Final spectra are shown in Figure 5. Details of the $H\alpha$ line profile are shown in Figures 6 and 7.

Table 3 also lists approximate emission equivalent widths (positive values for emission lines) of the $H\alpha$ line at each epoch ($W_{H\alpha}$). The uncertainty here is a few to 5%, dominated by the uncertainty in the continuum level (we could not measure an equivalent width for the 2011 Jan. 13

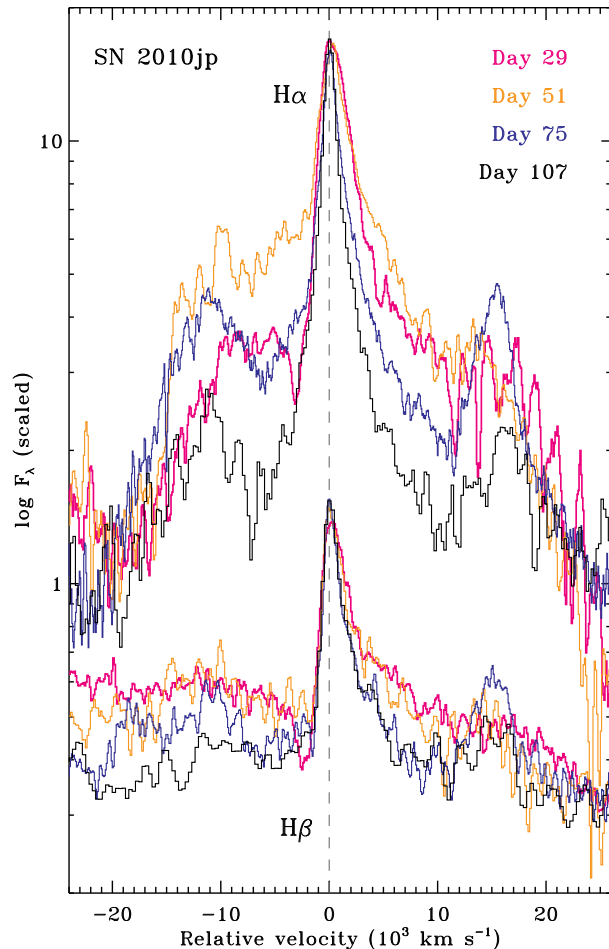


Figure 6. Evolution of the $H\alpha$ and $H\beta$ profiles of SN 2010jp.

spectrum from the MMT, since this high-resolution spectrum did not include the continuum on the blue side of the very broad line). Adopting a single value for the red continuum at each spectral epoch by fitting a straight line to the declining r and R magnitudes in Figure 3, we then converted these equivalent widths to total fluxes in the $H\alpha$ line. Figure 8 compares the decline rate of the continuum to the total $H\alpha$ line flux, as well as the flux of the high-velocity red bump component measured in the same spectra (we could measure the red component flux in the MMT spectrum). The total $H\alpha$ line flux declines more slowly with time compared to the red continuum, so that the equivalent width increases, as is typical for SNe II. However, from Figure 8 we also see that the high-velocity red bump increases its relative strength compared to the total line flux and continuum after day ~ 60 .

4 ANALYSIS

4.1 Light Curve and Luminosity

After reaching its peak luminosity at 20–30 days, SN 2010jp has a linear decline rate in visual-wavelength bands that is similar to SNe II-L and II-n, and does not show a plateau akin to SNe II-P (Figure 3). There is, however, tentative

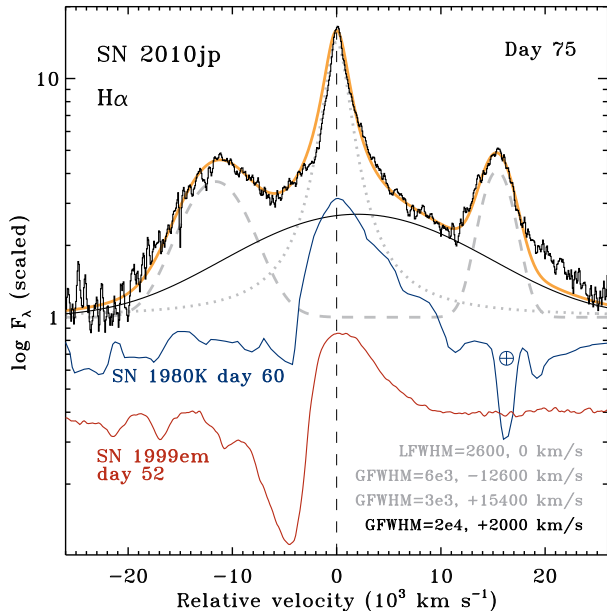


Figure 7. The $H\alpha$ profile of SN 2010jp on day 75, decomposed into multiple contributing features (thin black and grey curves) with the sum of all individual components shown in orange. GFWHM and LFWHM denote Gaussian or Lorentzian FWHM values and centroid velocities. For comparison, we also show the $H\alpha$ profile of the normal SN II-P 1999em from Leonard et al. (2002), plotted in red, as well as the $H\alpha$ line in the Type II-L SN 1980K observed on day ~ 60 (Barbieri et al. 1982) in blue (the absorption feature marked \oplus in the SN 1980K spectrum is an uncorrected telluric feature).

evidence for an increased fading rate after day 110, which is similar to some SNe IIn, such as SN 1994W (Sollerman et al. 1998). Linear fading is not unusual in the light curves of moderate-luminosity SNe IIn. A well studied example is SNe 1998S (Fassia et al. 2000), shown in Figure 3 for comparison. Other examples of moderate-luminosity SNe IIn with linear declines are SN 2005gl (Gal-Yam, et al. 2007), SN 2005ip (Smith et al. 2009b), and PTF09uj (Ofek et al. 2010). In general, the UVOT filters (Figure 4) show a somewhat faster decline rate than the R -band, which is typical for blue/UV decline rates of Type II SNe. This implies that the UV filters are dominated by continuum emission from the photosphere in the SN ejecta, and not CSM interaction.

SN 2010jp is sub-luminous compared to most SNe II-P, II-L, and IIn. While its overall light curve shape is quite similar to SN 1998S (Figure 3), it is about 2.5 mag fainter in terms of its absolute magnitude. It has a peak absolute magnitude of about -15.9 (unfiltered, approximately R -band), lying on the faint tail of the luminosity function for SNe IIn (Li et al. 2011). Note that in Figure 3, the apparent magnitudes of SN 1999em are shown as they would appear at the same distance and with the same reddening as SN 2010jp. In our spectra, we do not detect a strong narrow absorption component in Na I D, but Poznanski et al. (2011) find that the strength of Na I D is not a good proxy for line-of-sight extinction anyway. The characteristic visual-wavelength continuum temperature (after correcting for Galactic reddening) of ~ 6000 K is consistent with other SNe IIn, giving us no reason to suspect a value for the local reddening much

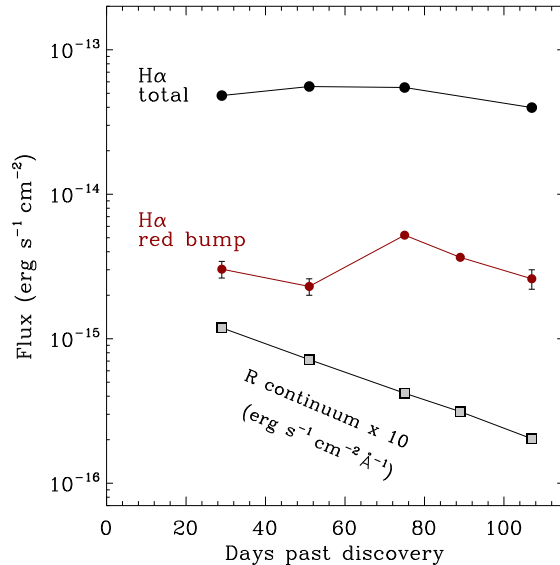


Figure 8. The total $H\alpha$ line flux (black dots) and the flux contained in just the red high-velocity component (red dots), as compared to the decline in the continuum flux over time (grey squares; flux density multiplied by a factor of 10 for display here). The error bars for the red component flux are shown, and the error bars for the total $H\alpha$ flux are smaller than the plotting symbols. These are measurement errors; there is also a $\sim 5\%$ uncertainty in the red continuum flux based on the smooth fit to the r and R -band magnitudes.

larger than about $A_V \simeq 0.5$ mag. Hence, we find it unlikely that the peak of SN 2010jp is more luminous than about -16 mag.

Since the peak luminosity is so low, we conjecture that CSM interaction does not provide a substantial luminosity boost for SN 2010jp. As such, the CSM interaction in SN 2010jp is similar to SNe IIn where the CSM interaction is strong enough to produce bright narrow emission lines in the spectrum, but where the CSM density is not high enough to provide efficient conversion of SN ejecta kinetic energy into continuum radiation (see Smith et al. 2009a). This implies that the progenitor star’s mass-loss rate was not more than about $10^{-3} M_{\odot} \text{ yr}^{-1}$ (Smith et al. 2009a). However, at late times (50-100 days) when SN 2010jp has faded from its peak luminosity, some of the variations in the light curve, if real, may be due to changes in the strength of CSM interaction as the shock overtakes density fluctuations in the CSM. Such changes may provide fluctuating contributions of UV continuum and line emission as the SN photosphere fades.

SN2010jp has a relatively low peak luminosity, but its low late-time luminosity is noteworthy as well. The luminosity indicated by the last two points after day 110 in Figure 2 would be consistent with a radioactive decay tail that is at least 10 times less luminous than that of SN 1999em. Adopting $M(^{56}\text{Ni}) = 0.03 M_{\odot}$ for SN 1999em ($0.02 M_{\odot}$ found by Elmhamdi et al. 2003, or $0.036 M_{\odot}$ from Utrobin 2007), this would imply an initial nickel mass less than about $M(^{56}\text{Ni}) \lesssim 0.003 M_{\odot}$ in SN 2010jp (see Figure 2), if increased extinction from newly formed dust can be neglected. This

is a very low nickel mass for a core collapse SN, comparable to that inferred for SN 1994W (although SN 1994W had a much higher peak luminosity; Sollerman et al. 1998). It could indicate either that the progenitor star had a relatively low initial mass near $8 M_{\odot}$, or that it was a substantially more massive star whose SN was underluminous because it lost much of the radioactive material into a black hole (see below).

4.2 Spectra

While the light curve for SN 2010jp is not very remarkable, its spectrum is quite unusual. The spectrum has a blue continuum with a characteristic temperature close to $\sim 6,000$ K, and strong Balmer lines that have narrow cores and broad wings (Figure 5). These properties are typical of some SNe IIn, especially those like SN 1988Z and SN 2005ip, where both a broad and narrow $H\alpha$ component can be seen clearly (Chugai & Danziger 1994; Smith et al. 2009b). In these SNe, the narrow Balmer emission is thought to arise from dense pre-shock circumstellar material (CSM) or material in a cold dense shell that has been hit by the forward shock, whereas the broader line components arise either in the freely expanding SN ejecta or the SN ejecta that have passed the reverse shock (see Chugai & Danziger 1994; Smith et al. 2008a, 2009b, 2010). Note, however, that broad line wings of a few 10^3 km s $^{-1}$ in SNe IIn can also arise from electron-scattering wings if they have the characteristic smooth Lorentzian profile (see Chugai 2001; Dessart et al. 2009; Smith et al. 2010). Thus, the most basic of SN 2010jp’s observed properties – the light curve shape and overall character of the spectrum – seem well-explained by a Type IIn supernova.

In our high-resolution MMT spectrum taken on day 89, the narrowest emission component of $H\alpha$ is fully resolved, with a Gaussian FWHM no narrower than about 800 km s $^{-1}$. This indicates circumstellar material that is considerably faster than the 100-200 km s $^{-1}$ speeds commonly observed in the CSM of some SNe IIn, but in line with the SNe IIn CSM velocities in the sample studied by Kiewe et al. (2010). Expansion speeds around 800 km s $^{-1}$ are much faster than can be achieved in a red supergiant wind, but such a speed is typical for the line widths observed in luminous blue variable (LBV)-like eruptions (Smith et al. 2011).

The key spectral feature of SN 2010jp that stands out compared to all other known SNe is that $H\alpha$ and other Balmer lines show fast blue and red emission bumps, yielding a pronounced *triple-peaked* line profile (see Figures 5 and 6). These triple peaks persist across multiple epochs during the first 100 days after explosion. They can be seen in higher Balmer lines like $H\beta$ (Figure 6), as well as $H\gamma$ and $H\delta$ (Figure 5), so the blue and red humps are definitely not contamination by unidentified emission lines on either side of $H\alpha$. These blue and red emission bumps are strong enough that in the higher order Balmer lines, they blend together to form an excess blue pseudo-continuum (Figure 5). Figure 7 breaks down the line profile into a narrow Lorentzian profile, a very broad Gaussian, and two well-defined Gaussian bumps centered at roughly $-13,000$ and $+15,000$ km s $^{-1}$, as indicated by our high signal-to-noise ratio spectrum on day 75. This is only meant to demonstrate that the blue and red humps are distinct, separate emission components. These bumps seem

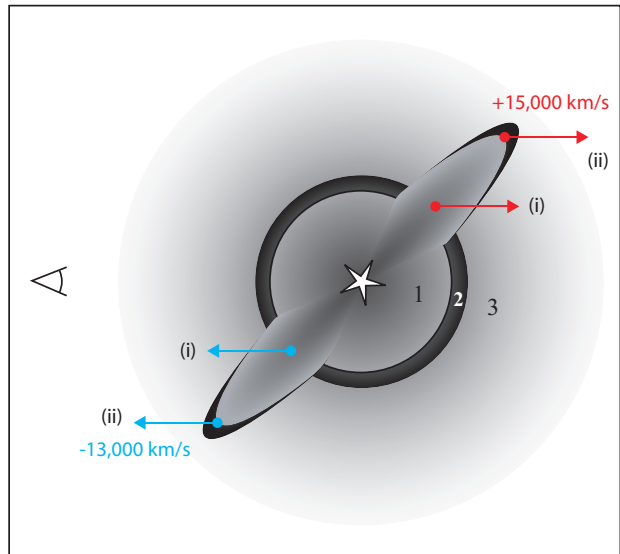


Figure 9. Cartoon of the possible jet-powered geometry in SN 2010jp. Regions 1, 2, and 3 correspond to the unshocked SN ejecta (inner gradient), the CSM interaction region (dark), and the pre-shock CSM (outer gradient), respectively. The upper-left and lower-right quadrants in this cartoon are the same as for a conventional SN IIn with CSM interaction, corresponding to low/mid-latitudes in the explosion. The lower-left and upper-right quadrants depict a tilted fast bipolar jet breaking through the otherwise spherical CSM interaction shell. An observer located to the left would see a combination of the spectrum from a conventional SN IIn, plus blue and red emission peaks in emission lines arising in either the unshocked jet material (i) or at the reverse shock in the jet (ii). We suggest that a bipolar jet such as this causes the blue and red bumps at $-13,000$ and $+15,000$ km s $^{-1}$ observed in the $H\alpha$ profile of SN 2010jp.

to shift slightly in velocity from one epoch to the next, but they do not stray far from those fiducial velocities, and the low signal to noise of some of the spectra make precise velocities difficult to measure. They do not, however, exhibit a systematic migration in velocity with time.

Figure 7 shows that the $H\alpha$ line wings and the blue and red emission humps in SN 2010jp are at very high speeds compared to those of prototypical SNe II-L and II-P (i.e. SNe 1980K and 1999em, respectively) at comparable epochs after explosion. The blue and red humps are also well separated from the central narrow/intermediate-width emission component, which by itself would not have been unusual, and the relative flux of the high-velocity components appears to fade at a rate that is different from the rest of the line (Figure 8; see below). This slow fading implies densities of $n_H \lesssim 10^6$ cm $^{-3}$ for the $H\alpha$ emitting region based on the expected cooling timescale.

At no time does the spectrum of SN 2010jp exhibit emission or absorption features associated with Fe II, and we do not see the IR Ca II triplet at late times that is usually seen in SNe II. Assuming that these features come from Ca and Fe that was present in the progenitor star’s envelope, this may be another indication of very low progenitor metallicity, as inferred from the SN host environment (see above).

5 DISCUSSION

We speculate that the observed properties of SN 2010jp can arise from a superposition of two physical scenarios. The first is a relatively traditional Type II_n explosion, where the rapidly expanding low-mass H envelope of the star collides with dense pre-existing CSM that was ejected recently by the progenitor. This can produce the blue continuum, the narrow emission cores of the Balmer lines, and some of the underlying broad emission profiles the same way that these arise in traditional SNe II_n (see, e.g., Chugai & Danziger 1994; Smith et al. 2008a, 2009b, 2010; Kiewe et al. 2010). We suspect that most of the emitting volume in SN 2010jp corresponds to this component (regions 1, 2, and 3 in Figure 9).

The second component superposed on this model is that SN 2010jp also produces a fast bipolar jet, tilted out of the plane of the sky, which gives rise to the fast blue and red emission features in H α , and may produce some of the emission in the very broad wings of the line. The combination of these two scenarios is depicted schematically in Figure 9.

We argue that the two isolated red and blue emitting components must arise in a collimated geometry. If the fast and slow components arose in a spherical geometry (i.e., a fast blast wave overrunning slow clumps; Chugai & Danziger 1994; Smith et al. 2009b), this would yield both broad and narrow components, but the fast material would form a broad component distributed over all velocities, not in blue and red peaks. Similarly, the reverse shock of fast ejecta plowing into a dense slow equatorial ring (as seen presently in SN1987A; Michael et al. 2003; Smith et al. 2005) would produce emission spread over all velocities if it is spatially unresolved. Two distinct, nearly symmetric blue and red components argue for a jet, because this can produce fast emitting material at very specific velocities, separated from the rest of the emitting ejecta (Figure 9). In hindsight, it would obviously have been useful to obtain spectropolarimetry of SN 2020jp to put additional constraints on the asymmetry (Wang & Wheeler 2008), but unfortunately we did not obtain these data.

The detection of a collimated jet in a Type II explosion is unprecedented. Models of jet-powered SNe have been published for fully stripped-envelope progenitors, which yield SNe Ibc and GRBs. Theoretical models also predict jet-driven SNe II for a wide range of initial masses exceeding $25 M_{\odot}$ (e.g., Heger et al. 2003), from collapsars that yield black holes. These are expected to be more common at sub-solar metallicity (Heger et al. 2003), due to the expectation of weaker metallicity-dependent mass loss. However, no clear case of a jet-driven SN II has yet been seen. For normal red supergiants (RSGs) with massive H envelopes, one expects that the collimated jet is largely destroyed while imparting its kinetic energy to a spherical envelope (MacFadyan et al. 2001; Höflich et al. 2001; Wheeler et al. 2002; Couch et al. 2009). It would be interesting to conduct similar hydrodynamic and radiative transfer simulations for a jet-driven SN from a progenitor that had a very small residual H envelope, perhaps due to the same type of episodic pre-SN mass loss that leads to a Type II_n event. This type of episodic mass loss may be driven by continuum radiation opacity or may be hydrodynamic, and is therefore not necessarily sensitive to metallicity (Smith & Owocki 2006). For a very small

amount of H remaining on the star’s surface, the jet might survive traversal of the envelope.

We consider two possible specific mechanisms that may power the emission in the fast blue and red peaks of the H Balmer series:

(i) A jet-powered explosion might mix significant quantities of ^{56}Ni to high velocities in the polar regions of a thin H envelope. The radioactivity would then heat that H-rich ejecta directly at those high velocities. In fact, it is interesting that the H α profile we observe in SN 2010jp bears a striking resemblance to the distribution of ^{56}Ni velocities in simulations of jet-powered SNe (Couch et al. 2009; see their Figure 12). A similar mechanism was proposed to explain similar (although much weaker) features in the H α profiles of the SNe II-P 1999em and 2004dj (Chugai et al. 2005; Elmhamdi et al. 2003). The lack of prominent Fe lines in the late-time spectrum may be a concern for this hypothesis, however.

(ii) Alternatively, without ^{56}Ni mixed to high velocities, the fast blue and red H α bumps may be excited by CSM interaction. Fast H-bearing SN ejecta that cross the reverse shock of the jet will also yield two very fast but localized velocity components (Figure 9). This option is difficult to rule out, given the evidence for CSM interaction in the Type II_n spectrum.

Choosing between these two will require additional theoretical work, including hydrodynamic radiative transfer simulations of jets in a light H envelope. Both of these require some H to be present at high velocities in the polar regions of the SN ejecta; therefore, a model wherein H only exists in the CSM (i.e., with a true stripped-envelope SN Ibc and jet plowing into dense H-rich CSM) cannot explain the observations of SN 2010jp. This may present an interesting challenge to current models of jets in core-collapse SNe.

Examining Figure 8, we see that at times after 50–60 days, the strength of the red high-velocity emission component (and also the blue component; not shown) appears to increase relative to that of the total H α line flux of the continuum flux density. This may mark the time when the recombination photosphere recedes through the faster parts of the ejecta to reveal the jet material heated radioactively in scenario (i), or when the fast jet overtakes and breaks through the optically thick CSM interaction shell in scenario (ii). The size of the ~ 6000 K continuum photosphere at this time should be very roughly 30 AU.

From our observations, it is not obvious if the jet in SN 2010jp was driven by accretion onto a newly born black hole or by a magnetar jet. Models of magnetar outflows colliding with SN ejecta have been invoked as a possible origin for some of the most luminous SNe known (Kasen & Bildsten 2010; Woosley 2010), but in SN 2010jp we see evidence for a collimated jet in a relatively *faint* SN with only moderate CSM interaction. We showed earlier that the peak absolute magnitude of SN 2010jp was 1–3 mag less luminous than typical SNe II-L and II_n, and that the late-time luminosity suggests a very small initial nickel mass of $M(^{56}\text{Ni}) \lesssim 0.003 M_{\odot}$. One might speculate that a weak explosion or small yield of ^{56}Ni might be the consequence of fallback into a black hole in a Type II collapsar, where some material from the accretion disk is launched poleward to produce the jets we observe. Jet-driven SNe II from collapsars can be more

energetic than normal SNe, but not necessarily (MacFadyan et al. 2001; Heger et al. 2003).

The radio and X-ray non-detections we report for SN 2010jp are, unfortunately, not very constraining in terms of choosing between options (i) and (ii) above. Type II_n SNe can have strong radio and X-ray emission from CSM interaction at late times, as in the case of SN 1988Z (Van Dyk et al. 1993; Fabian & Terlevich 1996; Schlegel & Petre 2006), but the radio and X-ray emission from CSM interaction can also be quashed due to high optical depths, as in the case of SN 2006gy (Smith et al. 2008b, 2010; Ofek et al. 2007). From the radii and density quoted above for SN 2010jp, the 1 GHz free-free continuum optical depth would be about 10^{20} .

Lastly, we consider the possibility that SN 2010jp was due to a transient accretion event where the fast blue and red emission bumps in the H α profile could be produced by a rotating disk around a massive black hole, akin to the class of active galactic nuclei that are double-peaked emitters (Halpern & Filippenko 1988). In order for the emitting radius of this fast orbiting material to be larger than the continuum photospheric radius required for SN 2010jp (about 20–60 AU at various times as the SN fades), the black hole mass would need to be more than $5 \times 10^6 M_{\odot}$. Such an event might resemble Sw 1644+57; Bloom et al. (2011a) proposed this to be a tidal disruption event around a 10^6 – $10^7 M_{\odot}$ black hole, whereas Quataert & Kasen (2011) discussed an alternative involving a weak SN/GRB event. Sw 1644+57 is coincident with the light centroid of its host galaxy, consistent with the possibility of a massive black hole. However, SN 2010jp’s location far outside a galactic nucleus and the non-detection of X-ray or radio emission make the tidal disruption hypothesis seem unlikely in this case. In addition, we should expect both the velocity of the blue and red peaks and the continuum temperature to increase with time in this scenario, as the photosphere recedes to reveal faster and hotter material in an accretion disk around the massive black hole. This behavior is not observed in SN 2010jp.

ACKNOWLEDGMENTS

We thank P. Challis and R. Kirshner for assistance with the MMT observations on 2010 November, and for providing the reduced spectrum from that night. S.B.C. acknowledges generous financial assistance from Gary & Cynthia Bengier, the Richard & Rhoda Goldman Fund, NASA/*Swift* grants NNX10AI21G and GO-7100028, the TABASGO Foundation, and NSF grant AST-0908886. D.P. and E.O.O. are supported by Einstein fellowships from NASA. The National Energy Research Scientific Computing Center, which is supported by the Office of Science of the U.S. Department of Energy under Contract No. DE-AC02-05CH11231, provided staff, computational resources, and data storage for this project. The Weizmann PTF partnership is supported in part by grants from the Israeli Science Foundation (ISF) to A.G. Collaborative Caltech-WIS work is supported by a grant from the Binational Science Foundation (BSF) to A.G. and S.R.K. The work of A.G. is further supported by an FP7 Marie Curie IRG Fellowship and the Benozio Center for Astrophysics, and by the Lord Sieff of Brimpton Memorial Fund. J.S.B. was partially supported by a grant from the National Science Foundation (NSF-CDI # 0941742). Some of the data presented herein were obtained at the W.M. Keck Observatory, which is operated as a scientific partnership among the California Institute of Technology, the University of California and the National Aeronautics and Space Administration. The Observatory was made possible by the generous financial support of the W.M. Keck Foundation. The authors wish to

recognize and acknowledge the very significant cultural role and reverence that the summit of Mauna Kea has always had within the indigenous Hawaiian community. We are most fortunate to have the opportunity to conduct observations from this mountain. The National Radio Astronomy Observatory is a facility of the National Science Foundation operated under cooperative agreement by Associated Universities, Inc.

REFERENCES

- Abazajian, K.N., et al. 2009, *ApJS*, 182, 543
 Arcavi, I., et al. 2010, *ApJ*, 721, 777
 Barbieri, C., Bonoli, C., & Cristiani, S. 1982, *A&A*, 114, 216
 Blondin, J., J.M., Mezzacappa, A., & DeMarino, C. 2003, *ApJ*, 584, 971
 Bloom, J.S., et al. 2011a, *Science*, 333, 203
 Bloom, J.S., et al. 2011b, arXiv:1106.5491
 Bodenheimer, P., & Ostriker, J.P. 1974, *ApJ*, 191, 465
 Bucciantini, N., Thompson, T.A., Aarons, J., Quataert, E., & Del Zanna, L. 2006, *MNRAS*, 368, 1717
 Buras, R., Rampp, M., Janka, H.T., & Kifonidis, K. 2006a, *A&A*, 447, 1049
 Buras, R., Janka, H.T., Rampp, M., & Kifonidis, K. 2006b, *A&A*, 457, 281
 Burrows, D.N., et al. 2005, *Space Science Rev.*, 120, 165
 Burrows, A., Livne, E., Dessart, L., Ott, C.D., & Murphy, J. 2006, *ApJ*, 640, 878
 Burrows, A., Dessart, L., Livne, E., Ott, C.D., & Murphy, J. 2007, *ApJ*, 664, 416
 Buta, R.J. 1982, *PASP*, 94, 578
 Butler, N. 2007, *AJ*, 133, 1027
 Cenko S.B., et al. 2006, *PASP*, 118, 1396
 Challis, P., Kirshner, R., & Smith, N. 2010, *CBET*, 2548, 1
 Chornock, R., et al. 2011, arXiv:1001.2775
 Chugai, N.N., & Danziger, I.J., 1994, *MNRAS*, 268, 173
 Chugai, N.N., Fabrika, S.N., Sholukhova, O.N., Goranskij, V.P., Abolmasov, P.K., & Vlasjuk, P.P. 2005, *Astron. Lett.*, 31, 792
 Couch, S.M., Wheeler, J.C., & Milosavljević, M. 2009, *ApJ*, 696, 953
 Dessart, L., Burrows, A., Livne, E., & Ott, C.D. 2008, *ApJ*, 673, L43
 Dessart, L., Hillier, D.J., Gezari, S., Basa, S., & Matheson, T. 2009, *MNRAS*, 394, 21
 Elmhamdi, A., et al. 2003, *MNRAS*, 338, 939
 Fabian, A.C., & Terlevich, R. 1996, *MNRAS*, 280, L5
 Fassia, A., et al. 2000, *MNRAS*, 318, 1093
 Elmhamdi, A., et al. 2003, *MNRAS*, 338, 939
 Filippenko, A.V. 1982, *PASP*, 94, 715
 Galama, T.J., et al. 1998, *Nature*, 395, 670
 Gal-Yam, A., et al. 2004, *ApJ*, 609, L59 L62
 Gal-Yam, A., et al. 2007, *ApJ*, 356, 672
 Gal-Yam, A., Maoz, D., Guhathakurta, P., and Filippenko, A.V. 2008, *ApJ*, 680, 550
 Gal-Yam, A., et al. 2011, arXiv:1106.0400
 Gehrels, N., et al. 2004, *ApJ*, 611, 1005
 Halpern, J. P., & Filippenko, A. V. 1988, *Nature*, 331, 46
 Höflich, P.A., Kholkov, A., & Wang, L. 2001, in 20th Texas Symp. on Relativistic Astroph., eds. J.C. Wheeler, & H. Martel (New York: AIP), 459
 Jeffery, D.J. 1991, *ApJS*, 77, 405
 Jordi K., Grebel E. K., Ammon K., 2006, *A&A*, 460, 339
 Kasen, D., & Bildsten, L. 2010, *ApJ*, 717, 245
 Kiewe, M., et al. 2010, arXiv:1010.2689
 Khokhlov, M., Höflich, P.A., Oran, E.S., Wheeler, J.C., Wang, L., & Chitchekanova, A.Y. 1999, *ApJ*, 524, L107
 Komissarov, S.S., & Barkov, M.V. 2007, *MNRAS*, 382, 1029
 Law, N.M., et al. 2009, *PASP*, 121, 1395
 LeBlanc, J.M., & Wilson, J.R. 1970, *ApJ* 161, 541
 Leonard, D. C., Filippenko, A.V., Barth, A.J., & Matheson, T. 2000, *ApJ*, 536, 239
 Leonard, D.C., Filippenko, A.V., Ardila, D.R., & Brotherton, M.S. 2001, *ApJ*, 553, 861
 Leonard, D. C., et al. 2002, *PASP*, 114, 35
 Leonard, D. C., et al. 2006, *Nature*, 440, 505
 Li, W., Jha, S., Filippenko, A.V., Bloom, J.S., Pooley, D., Foley, R.J., & Perley, D.A. 2006, *PASP*, 118, 37
 Li, W., et al. 2011, *MNRAS*, 412, 1441
 MacFadyen, A.I., & Woosley, S.E. 1999, *ApJ*, 524, 262
 MacFadyen, A.I., Woosley, S.E., & Heger, A. 2001, *ApJ*, 550, 410
 Maeda, K., & Nomoto, K. 2003, *ApJ*, 598, 1163
 Matheson, T., et al. 2003, *ApJ*, 599, 394
 Maza, J., et al. 2010, *CBET*, 2544, 1
 Mazzali, P.A., et al. 2005, *Science*, 308, 1284
 Metzger, B.D., Giannios, D., Thompson, T.A., Bucciantini, N., & Quataert, E. 2010, arXiv:1012.0001
 Michael, E., et al. 2003, *ApJ*, 593, 809

- Monet, D.G., et al. 2003, AJ, 125, 984
- Ofek, E.O., et al. 2007, ApJ, 659, L13
- Ofek, E.O., et al. 2010, ApJ, 724, 1396
- Oke, J.B., & Gunn, J.E. 1982, PASP, 94, 586
- Oke, J.B., & Gunn, J.E. 1983, ApJ, 266, 713
- Oke, J.B., et al. 1995, PASP, 107, 375
- Perley, R., et al. 2009, IEEE Preceedings, 97, 1448
- Poole, T.S., et al. 2008, MNRAS, 383, 627
- Poznanski, D., Ganeshalingam, M., Silverman, J., & Filippenko, A.V. 2011, MNRAS, 415, L81
- Quataert, E., & Kasen, D. 2011, MNRAS, submitted (arXiv:1105.3209)
- Rahmer G., Smith R., Velur V., Hale D., Law N., Bui K., Petrie H., & Dekany R. 2008, in Society of Photo- Optical Instrumentation Engineers (SPIE) Conference Series Vol. 7014 of Presented at the Society of Photo-Optical Instrumentation Engineers (SPIE) Conference
- Rau, A., et al. 2009, PASP, 121, 1334
- Roming, P.W.A., et al. 2005, Space Sci. Rev., 120, 95
- Schlegel, D.J., Finkbeiner, D.P., & Davis, M. 1998, ApJ, 500, 525
- Schlegel, E.M., & Petre, R. 2006, ApJ, 646, 378
- Smith, N., & Owocki, S.P. 2006, ApJ, 645, L45
- Smith, N., Zhekov, S.A., Heng, K., McCray, R., Morse, J.A., & Gladders, M. 2005, ApJ, 635, L41
- Smith, N., Chornock, R., Li, W., Ganeshalingam, M., Silverman, J.S., Foley, R., Filippenko, A.V., & Barth, A.J. 2008a, ApJ, 686, 467
- Smith, N., et al. 2008b, ApJ, 686, 485
- Smith, N., Hinkle, K.H., & Ryde, N. 2009a, AJ, 137, 3558
- Smith, N., et al. 2009b, ApJ, 695, 1334
- Smith, N., et al. 2010, ApJ, 709, 856
- Smith, N., et al. 2011, MNRAS, in press (arXiv:1010.3718)
- Sollerman, J., Cumming, R.J., & Lundqvist, P. 1998, ApJ, 493, 933
- Thompson, T.A., Chang, P., & Quataert, E. 2004, ApJ, 611, 380
- Trammell, S.R., Hines, D.C., & Wheeler, J.C. 1993, ApJ, 414, L21
- Tran, H.D., Filippenko, A.V., Schmidt, G.D., Bjorkman, K.S., Jannuzi, B.T., & Smith, P.S. 1997, PASP, 109, 489
- Utrobin, V.P. 2007, A&A, 461, 233
- Van Dyk, S.D., Weiler, K.W., Sramek, R.A., & Panagia, N. 1993, ApJ, 419, L69
- Wang, L., & Wheeler, J.C. 2008, ARAA, 46, 433
- Wang, L., Howell, A., Höflich, P., & Wheeler, J.C. 2001, ApJ, 550, 1030
- Wheeler, J.C., Yi, I., Höflich, P., & Wang, L. 2000, ApJ, 537, 810
- Woosley, S.E. 2010, ApJ, 719, L204
- Woosley, S.E., & Bloom, J.S. 2006, ARAA, 44, 507